

Perfect coupling of light to surface plasmons with ultra-narrow linewidths

M. Sukharev^{1*}, P. R. Sievert², T. Seideman³, and J. B. Ketterson^{2,4}

¹*Department of Applied Sciences and Mathematics,
Arizona State University at the Polytechnic Campus, Mesa AZ, 85212, USA*

²*Department of Physics and Astronomy,
Northwestern University, Evanston IL, 60208, USA*

³*Department of Chemistry, Northwestern University, Evanston IL, 60208, USA*

⁴*Department of Electrical and Computer Engineering,
Northwestern University, Evanston IL, 60208, USA*

**corresponding author: maxim.sukharev@asu.edu*

Abstract

We examine the coupling of electromagnetic waves incident normal to a thin silver film that forms an oscillatory grating embedded between two otherwise uniform, semi-infinite half spaces. Two grating structures are considered, in one of which the mid point of the Ag film remains fixed whereas the thickness varies sinusoidally, while in the other the mid point oscillates sinusoidally whereas the film thicknesses remains fixed. On reducing the light wavelength from the long wavelength limit, we encounter signatures in the transmission, T , and reflection, R , coefficients associated with: i) the short-range surface plasmon mode, ii) the long-range surface plasmon mode, and iii) electromagnetic diffraction tangent to the grating. The first two features can be regarded as generalized (plasmon) Wood's anomalies whereas the third is the first-order conventional (electromagnetic) Wood's anomaly. The energy density at the film surface is enhanced for wavelengths corresponding to these three anomalies, particularly for the long range plasmon mode in thin films. When exciting the silver film with a pair of waves incident from opposite directions, we find that by adjusting the grating oscillation amplitude and fixing the relative phase of the incoming waves to be even or odd, $T + R$ can be made to vanish for one or the other of the plasmon modes; this corresponds to perfect coupling (impedance matching in the language of electrical engineering) between the incoming light and these modes.

I. INTRODUCTION

There is currently much interest in the physical properties and possible applications of plasmons excited in various metallic structures [1, 2, 3, 4, 5, 6, 7], particularly those made from silver or gold, where relatively narrow resonances are observed relative to some other metals [8]. Much of this interest is associated with the high electric fields generated by various resonant responses. Common among the many applications of these fields is the enhancement of nonlinear optical responses for optical devices [9] or spectroscopic applications [10]. The simplest plasmonic structure is a single metallic sphere. In the limit where the sphere diameter is small compared to the wavelength of the incident light, the polarization is well described by the leading term in the Mie expansion, corresponding to a single peak at $\omega = \omega_{bp}/\sqrt{3}$, where ω_{bp} is the bulk plasmon frequency [11]. As the sphere size increases higher order terms in the Mie expansion become important [12].

Smaller sphere radii yield larger field enhancements at the particle surface. For ellipsoids [13], when the exciting field lies along the major axis of a prolate ellipsoid of revolution, the high curvature for the surface normal to that direction further enhances the field; this is the so-called lightning rod effect. One is then encouraged to examine structures with sharp corners, such as pyramids [14], or assemblies of these containing adjacent sharp corners leading to higher local field enhancements. Although the local fields associated with small finite structures and their arrays can be relatively high, they are in practice limited by various effects including boundary scattering and radiation losses. With regard to the latter, one is encouraged to examine structures where radiation is suppressed.

The specific case of surface plasmons has long been studied [15]. When propagating at a half space separating a bulk metal from an adjacent dielectric, radiation is kinematically forbidden; damping only involves scattering from inhomogeneities (e.g. a rough surface) and dissipation in the metal itself. In fact the very existence of a surface plasmon requires that its frequency, ω_p , and wavevector, k_p , not match light propagating at any angle in the surrounding dielectric. For this reason it is common to couple to surface plasmons via an evanescent light wave and carefully control the coupling strength. In the commonly used Otto geometry [16] this is accomplished by forming a thin dielectric layer between a prism and the free surface of the metal adjacent to it. By adjustment of the thickness of the coupling layer, the reflected beam in the prism can be made to vanish at some critical angle

[17], a condition we will refer to as *critical coupling*.

If, in the Otto geometry, the metal layer (generally a vapor deposited thin film) has a finite thickness, plasmons involving both sides can be excited. If the dielectric constant of the coupling layer and that of the far side differ, modes with different wavelengths for a given frequency are present, which tend to localize on opposing sides of the metal film. When the dielectric constants on both sides are identical, however, the modes become degenerate; if in addition the film is thin, the modes are strongly coupled and split, with one being symmetric and the other antisymmetric with respect to the mid point of the film [15]. The structure of these modes was first examined by Economou [18]. Later work by Sarid [19] showed that the damping of the symmetric modes is greatly reduced as the film thins leading to long range propagation; the antisymmetric mode turns out to have a much shorter range.

This paper focuses on coupling to the long- and short-range modes using a sinusoidal grating for the case of perpendicular incidence involving a special case of Wood's anomaly, which we discuss at greater length below. Grating coupling has been used to experimentally couple to plasmon modes at a free surface, in connection with a study of the associated one-dimensional plasmon bandstructure [20]. More recently the plasmon bandstructure for thin square-wave modulated films has been examined [5]. Structures similar to those modeled here have recently been studied experimentally and will be reported elsewhere [21]. On the practical side, when coupled with an appropriate dye, the structures may be used to make future vertically emitting plasmonic band-gap lasers [22].

The paper is arranged as follows. In Section II we consider electromagnetic modes in the Otto geometry in symmetric dielectric environments modeled with a dielectric constant, $\varepsilon_{Ag}(\omega)$ corresponding to silver embedded in a water environment. We also present calculations of intensity enhancements and line widths for critical coupling. Section III describes the methodology applied in our numerical simulations and illustrates results for in-phase and out-of-phase oscillatory gratings using the same silver and dielectric environment parameters used for the Otto geometry simulations. Specifically, we calculate surface averaged field enhancements, demonstrating large enhancements at the Wood's anomalies, in particular for the long-range mode. Our conclusions are summarized in Section IV.

II. LONG- AND SHORT-RANGE PLASMONS IN THIN, FLAT METAL FILMS

Although the magnetic field amplitude is largest within the metal for the symmetric mode, the corresponding electric field has a node at the mid point and its over-all amplitude is smaller than for the antisymmetric mode; hence it has a smaller dissipation, leading to a longer range (and correspondingly a longer lifetime). One of our goals in the present study is to achieve the largest possible electric field enhancements in a spatially resonant, film-based structure and therefore low dissipation is a desirable feature. We will refer to this symmetric mode as the *long-range plasmon*. In addition the energy density lies largely outside the film, with the result that the mode velocity approaches that of light in the surrounding dielectric as the film is thinned [15]; the mode can be thought of as being “stiff” in this sense.

On the other hand the electric field for the antisymmetric mode is, over-all, larger within the metal. This leads to greater damping as the film is thinned; simultaneously the velocity falls (being “loaded” by the metal) and the mode is “soft” in this sense. We therefore refer to this mode as the *short-range plasmon*.

In modeling the overall behavior of the incoming beam in an Otto geometry experiment, one can regard the system as a stack of dielectric layers and apply the Fresnel conditions at all interfaces, while simultaneously accounting for the propagation between interfaces. In the present study, we consider a silver film and approximate the dielectric function by the Drude model,

$$\varepsilon_1(\omega) = \varepsilon_\infty - \frac{\omega_{bp}^2}{(\omega^2 + i\omega\Gamma)} \quad (1)$$

where the parameters are $\omega_{bp} = 1.7901 \times 10^{16}$ rad/sec, $\Gamma = 3.0841 \times 10^{14}$ rad/sec, and $\varepsilon_\infty = 8.926$. This model is a good representation of silver films for wavelengths between 300 nm and 700 nm. We define $k_0 = 2\pi/\lambda_0 = \omega/c$, the wave vector of the exciting light of wavelength λ_0 in vacuum, where c is the velocity of light. For very thin films the effects of scattering from an additional boundary would enter; no attempt to incorporate such effects is made in what follows. Note the effects of scattering from a single boundary are implicitly contained in the measured reflectivity data from which the dielectric constant is obtained.

Using dispersion relations for the plasmon modes in the Sarid geometry and our model parameters one can show that the high (long-range) and low (short-range) frequency modes lie, respectively, above and below that for a surface plasmon propagating at a half space,

where the latter is given by

$$\frac{\omega}{\omega_{bp}} = \frac{1}{\sqrt{\varepsilon_\infty + \varepsilon_2}}, \quad (2)$$

here we will take the dielectric constant of the host medium, ε_2 , is 1.76, corresponding to water. Eq. (2) results in 0.306 for our model parameters. Both families of curves approach this limit as the film thicknesses increases. This indicates the validity of our solution, although it is not strictly within the range of applicability of the Drude model. We also note that as the real in-plane plasma momentum decreases, all curves merge with the "light-line" for the dielectric medium, which is given by $(\omega/\omega_{bp}) = (1/\sqrt{\varepsilon_2})(k'_\rho/k_{bp})$; here k_{bp} is the in-plane wave vector of the bulk plasmon and k'_ρ is the real part of the in-plane complex wave vector of the plasmon. As it was found in [19], the high frequency mode has a very long range for thin films. As noted above, this is due to destructive interference of the overlapping evanescent fields in the metal, which minimizes the energy dissipation for this mode and enhances the lifetime of the plasmons at the surface. The dissipation decreases quadratically with the film thickness and linearly with the imaginary part of ε_1 .

For the purpose of our paper it is desirable to couple into the long-range plasmon mode with the minimum radiation loss, as this should maximize the field strength on the metal film. For a featureless, flat, metal film and fixed excitation frequency, the only method available is "tuning", i.e. varying the thickness, of the dielectric (coupling) layer between the coupling prism and the metal film. The total reflection coefficient is then calculated from the generalized Fresnel coefficients, accounting for the multiple reflections from the layers involved. The incident light wavelength is swept while the nominal angle of incidence is varied to correspond to a fixed in-plane momentum k'_ρ of $(2\pi/400) \text{ nm}^{-1}$ (this fixed value of k'_ρ is arbitrary but corresponds to the periodicity of the grating couplers considered in Section III below). Excitation of the plasmon modes is indicated by minima in the total reflection. The minimum corresponding to either mode can be "tuned" to zero by adjusting the thickness of the dielectric layer. This is the critical coupling layer thickness and corresponds to perfect coupling or impedance matching. The energy reflection at critical coupling for the long-lived mode versus the wavelength for a number of silver film thicknesses is given in Fig. 1A. One can determine a linewidth at the half-power line at various film thicknesses and calculate the Q -factor, defined as $Q = \lambda/\Delta\lambda$. The results are shown in Fig. 1B. Note that the Q significantly increases as the silver layer thins and increases by 4 orders of magnitude at a thickness of 5 nm, implying a corresponding build up of the stored

energy; the electric field, which scales as the square root of the energy density, is similarly enhanced.

III. OPTICS OF METAL GRATINGS AT IMPEDANCE MATCHING CONDITIONS

An alternative way of coupling into surface plasmons is to arrange for the metal film to act as a diffraction grating, a "line grating" in the present study. The choice of the grating structure introduces a wide range of physical scenarios. A relatively simple choice involves a sinusoidal variation of the position of the metal/dielectric interfaces and here we will study two limiting cases the two limiting cases shown in Figs. 2A, B. In Fig. 2A the mid point of the metal film remains fixed but the thickness varies sinusoidally between values $2D_1$ and $2D_2$ [23]; in Fig. 2B we have a case where the mid point oscillates sinusoidally with amplitude $2D_2$ but the film thicknesses remains fixed at a value $2D_1$. The two sinusoids are, respectively, out-of-phase and in-phase for these two cases, as shown in Fig. 2A. Intuitively we expect the modes for the constant thickness case to closely resemble the Sarid modes on a flat film while simultaneously allowing grating coupling to an external light wave.

For an incoming direction and wavelength for which the grating diffracts the light tangent to the grating, such that the diffracted wave is "in step" with the grating itself, one expects a stronger coupling; this enhanced interaction manifests itself as anomalies in other diffracted orders including the zeroth-order transmitted, T , and reflected, R , light intensity. Note that when energy is absorbed by the film, the condition $T + R = 1$, which one would have for a stack of lossless dielectric layers, does not apply. The phenomena, first discovered by R. W. Wood, is referred to as *Wood's anomaly*; the theoretical explanation was first given by Rayleigh and for this reason it is also called the Rayleigh-Wood anomaly. For a rigorous discussion the reader is referred to reference [24].

The Wood's phenomena is shown schematically in Fig. 3 for the case of a wave entering perpendicular to the grating. In this case we have equal and opposite diffracted waves (for a total of two, unlike the case for an arbitrary incident angle) that form a standing wave, and one may anticipate an even stronger interaction.

As a generalization of the Rayleigh-Wood phenomena, we will include the two cases where the wavelength of the long- and short-range plasmons (rather than the electromagnetic wave)

matches the grating spacing, which we can interpret as *plasmon Wood's anomalies*. We note in passing that when the incoming wave is perpendicular to the film one couples to the plasmons at the second Brillouin zone point of the associated one-dimensional plasmonic band structure within the film that is associated with the presence of the periodic grating.

The optical properties of the periodic metal structures depicted in the Fig. 2 were simulated using FDTD [25] in two dimensions. We have restricted ourselves to the case of normal incidence; furthermore we limit the calculations to the transverse magnetic mode, TM, which couples to plasmons propagating in the same direction as the static grating waves. For two dimensions this mode is sometimes designated as the transverse electric mode [25], TE_z , and has two electric and one magnetic component. The form given in Eq. (1), with identical parameters, forms the basis for the dielectric response of the metal to external EM excitation.

The FDTD unit cell used in the simulations is shown schematically in the Fig. 2B. The upper and lower parts of the grid are terminated by horizontal absorbing boundaries, for which we use perfectly matched layers (PML) [26] with a depth of 16 spatial steps and exponential differences in order to avoid diffusion instabilities. In all simulations we use a uniform Yee grid with spatial steps $\delta x = \delta y = 0.98$ nm and a time step $\delta t = \delta x / (1.5c)$. The metal film is assumed to be embedded in a dielectric with refractive index of 1.33, corresponding to $\epsilon_2 = 1.76$. We note that the latter leads to a Wood's anomaly at 532 nm for the 400 nm periodic gratings as discussed in the previous section. The gratings are excited by x -polarized plane waves that are generated along horizontal lines near the PML regions. All simulations have been performed in parallel using 128 processors on the DataStar cluster at the San Diego Supercomputer Center and Saguaro cluster at the ASU High Performance Computing Center. An average execution time of our codes is approximately 20 minutes or less.

Since the FDTD algorithm is a time domain integrator, electromagnetic (EM) field components at some pre-defined incident wavelength can be obtained either by applying a long excitation pulse, with duration much longer than the characteristic resonant lifetime, or by exciting the system with an ultra-short incident pulse and subsequently Fourier transforming the resulting EM fields. The latter method requires a single FDTD run within which one obtains the entire spectrum. Here we employ simulations of phasor functions using a discrete Fourier transform "on-the-fly" procedure with a short pulse excitation scheme [25, 27].

In order to calculate the transmission, T , and reflection, R , coefficients, we numerically integrate the Poynting vector normal to the horizontal lines shown in Fig. 2B as dashed lines. Transmission, T , is calculated using the total fields, which consists of the EM waves scattered by the metal film and the incident field, whereas reflection, R , is simulated using the scattered fields only, so as to exclude standing waves generated by interference between the incident field and the EM waves scattered back by the film. Numerical convergence is verified by ascertaining that $T + R = 1$ for a lossless dielectric for all wavelengths of interest. For the double-ended excitation scheme, i.e. for the case of excitation of the grating from both sides of the film, we perform simulations of the reflection for both sides of the structure using scattered fields only. Finally, in order to assure numerical convergence especially in the vicinity of sharp resonances we integrate Maxwell equations for as long as 2 ps.

Unlike the Otto geometry discussed above, we do not in general expect to be able to achieve critical coupling for our gratings, in the sense that all of the incoming energy is absorbed by the film; this would require two quantities to simultaneously vanish, namely the transmission and reflection coefficients, whereas we have only a single parameter, the amplitude of the grating oscillation, to vary (here we assume the thickness, or average thickness for the out-of-phase gratings, is held constant). For this reason we performed simulations where the beams simultaneously enter normal to the grating but from opposite sides. On symmetry grounds we anticipated that if these waves were in phase or out of phase we might selectively excite either the short-range or long-range plasmon modes, but not both; this was confirmed by the simulations, although the couplings for in-phase and out-of-phase sinusoids were reversed as will be discussed below. For such a case we then have only a single quantity, $T + R$, which has the same magnitude on both sides and simulations show that we may cause it to vanish (corresponding to critical coupling) at some critical value of our single grating amplitude parameter. We note that if the oscillation amplitudes on the upper and lower surfaces were independently varied (while maintaining constant average thickness), critical coupling should be achievable under single ended excitation, since we then have two independent parameters with which to simultaneously tune T and R through zero.

Fig. 4A shows simulations for an out-of-phase grating (see Fig. 2A) and calculate $T + R$ as a function of the free space incident wavelength, λ_0 , for three excitation schemes: i) single-ended excitation (solid line); ii) symmetric double-ended excitation (dash-dotted line)

(where two in-phase plane waves emanating from symmetrically placed horizontal lines near the upper and lower PML regions excite the metal); and iii) anti-symmetric double-ended excitation (dashed line) (which is similar to the symmetric scheme except that the phase difference between the two incident waves is π). The single-ended excitation scheme clearly generates all three modes: an electromagnetic Wood's anomaly located at $\lambda = 532$ nm and the long-range and short-range surface plasmon modes localized at 545 nm and 624 nm, respectively. We note that the resonant wavelength for the electromagnetic Wood's anomaly accurately corresponds to the grating period of 400 nm in the dielectric media with the refractive index of 1.33.

It is apparent in Fig. 4A that the phase delay between the two incident pulses in the double-ended excitation scheme gives us a control over the symmetry of the excited surface plasmon mode. The observed behavior can be summarized as follows: for the case of out-of-phase sinusoidal gratings (which are symmetric with respect to the film center), in-phase incoming waves excite the symmetric mode whereas out-of-phase waves excite the antisymmetric mode. On the other hand, Fig. 4B shows calculations for an in-phase sinusoidal grating where the converse is true: in-phase incoming waves excite the antisymmetric mode whereas out-of-phase waves excite the symmetric mode.

Provided that our gratings do not significantly depart from flat films, we expect the anti-symmetric and symmetric resonant wavelengths to be approximately given by the long- and short-range modes, which are governed by the film thickness as given in Fig. 1. For the in-phase gratings the thickness is given by $2D_1$ and we can then use the parameter $2D_2$ to control the coupling. For the out-of-phase sinusoids the resonant wavelength would, in the first approximation, be governed by the average thickness, $(D_1 + D_2)$; the difference, $(D_1 - D_2)$, can then be adjusted to control the coupling.

Fig. 4A shows an example of an out-of-phase sinusoidal grating described by the parameters $D_1 = 5$ nm and $D_2 = 31$ nm. Here we achieve a near perfect coupling for both the short- and long-range modes with the same parameter set. Note that with the single ended excitation the maximum coupling is approximately 50%. Fig. 4B shows an example of an in-phase grating where the parameters $D_1 = 10$ nm and $D_2 = 14.4$ nm minimize $T + R$ for the long-range surface plasmon mode. As discussed in previous sections, at the impedance matching conditions incident EM radiation is efficiently transformed into propagating surface plasmons leading to strong field enhancements on the surface of the gratings. Fig.

5A presents the intensity enhancement factors averaged over the metal surface for the out-of-phase (solid line) and in-phase (dashed line) sinusoidal grating under the double-ended excitation conditions (here we consider only long-range modes). We note that high EM fields, significantly enhanced at the impedance matching conditions, are not localized near specific spatial regions, as in the case of tip-enhanced optical probes [28], as expected for a standing sinusoidal wave. Following the results of Section II we simulated the enhancement for several grating thicknesses as shown in Fig. 5B. The results confirm our general conclusions that with thinner films the intensity enhancements are much higher as follows from the high quality factors Q (see Fig. 1B for details).

IV. DISCUSSION AND CONCLUSIONS

The above calculations demonstrate that the largest enhancements occur for the long-range mode for an in-phase oscillation of the grating amplitude. In evaluating nonlinear optics applications requiring rapid response, one must keep in mind that resonance is always accompanied by dispersion and the associated distortion of waveforms; the number of field cycles required to build up a response is proportional to the Q of the resonance and this may be particularly important when, e.g., trying to exploit plasmon waveguiding. Hence we envision the large enhancements obtained here would primarily be exploited for sensor applications.

We recall that the large intensity enhancements for our grating structures given in section III were calculated on a per-unit-area basis. This property is particularly important when considering sensor applications involving fluorescence-based spectroscopy or Surface Enhanced Raman Spectroscopy (SERS) where we assume we have no control over where the target molecule will actually attach. It is sometimes assumed that the enhancement of SERS scales as the square of the intensity; although this appears physically unreasonable, we note that the surface averaged square of the intensity is also greatly enhanced. Although various plasmon resonant nanostructures can have “hot spots” with rather large intensity enhancements, exploiting these requires that the target molecules “find” these hot spots, which in turn requires effective mixing or long exposure times. If receptors are involved one would want them attached only on the hot spots; if they are widely distributed they will compete with the hot spots for target molecules thereby depleting the latter.

Many other one-dimensional grating structures come to mind, including grooves and slots; both have multiple parameters (thickness, width, vertical position) associated with them, which can be tuned to achieve critical coupling under single ended excitation. The sharp edges associated with these structures can lead to further, but highly local, enhancements. Two-dimensional (e.g. hole) arrays are natural extensions. Our group is currently examining several of these structures. For SERS, and especially for fluorescence, the response of the grating at the emission (shifted) wavelength is also important, an issue under study.

In connection with possible SERS applications we point out that it should be possible to engineer one- and two-dimensional structures where light is i) gathered and ii) concentrated in a “two step” process involving a periodic array of bumps, ridges or holes. Firstly, the periodic grating structure so formed would be engineered to efficiently collect the light in an impedance matched manner, as we have described. Second, the edges of the structures so patterned would optimize to concentrate these fields.

We now discuss several technical issues regarding the implementation of the structures we have modeled. We used water for the dielectric in our simulations; i.e. we are implicitly assuming water-based sensor applications. In order to support the film, we require an insulating coating on a substrate whose dielectric constant can be adjusted to equal that of water. Such a material is Teflon AF[®] manufactured by Dupont. Although forming a sinusoidal grating is challenging, one can pattern and etch a grooved structure in, e.g., a glass or Si substrate by a variety of techniques, where the groove edges naturally develop a slope under simple etching protocols. Subsequently spinning on of Teflon AF would, via surface tension, further smooth the contour, thereby better approximating a sine wave. Depositing a uniform Ag film on a low surface tension material like Teflon AF may also be problematic. We note that silver reacts with water over time and so one might use Au (for which the enhancements will be lower) or spin on a very thin protective layer of Teflon AF over or within which any receptors would be incorporated [29].

Finally we must address the issue of matching the grating resonance frequency for the long-range mode to that of an available laser, say an argon (517 nm) or a YAG (532 nm) laser. Forming the structure with the required d -spacing is not an option, given the narrowness of the resonances. One can, however, take advantage of the degree of freedom mentioned in the Introduction, namely tipping the incoming laser beam out of the scattering plane, in particular in a direction parallel to the grating lines (corresponding to $\theta = \pi/2$). By

making the d -spacing slightly smaller than that which would match the resonance one can tune through the resonance by decreasing θ slightly from the plane normal. At resonance we would retain a standing wave along the grating plane and directed normal to its lines but the plasmon wavevector would then have a small component parallel to the lines.

Acknowledgments

This research was supported in part by the NCLT program of the National Science Foundation at the Materials Research Institute of Northwestern University (grant number ESI-0426328) and the AFOSR DARPA program (grant number FA9550-08-1-0221). The numerical work was enabled by the resources of the National Science Foundation San Diego Supercomputer Center under grant number MCA06N016.

-
- [1] S. A. Maier and H. A. Atwater, *J. App. Phys.* **98**, 011101 (2005).
 - [2] E. Ozbay, *Science* **311**, 189 (2006).
 - [3] F. J. Garcia de Abajo, *Rev. Mod. Phys.* **79**, 1267 (2007).
 - [4] H. F. Ghaemi, Tineke Thio, D. E. Grupp, T. W. Ebbesen, and H. J. Lezec, *Phys. Rev. B* **58**, 6779 (1998).
 - [5] T. Okamoto, J. Simonen and S. Kawata, *Phys. Rev. B* **77**, 115425 (2008).
 - [6] W. A. Murray and W. L. Barnes, *Adv. Mat.* **19**, 3771 (2007).
 - [7] P. B. Catrysse, *Nature Phys.* **3**, 839 (2007).
 - [8] A. M. Schwartzberg and J. Z. Zhang, *J. Phys. Chem. C* **112**, 10323 (2008).
 - [9] E. Hutter and J. H. Fendler, *Adv. Mat.* **16**, 1685 (2004).
 - [10] A. J Haes and R. P. Van Duyne, *Expert Rev. Mol. Diagn.* **4**, 527 (2004).
 - [11] U. Kreibig and M. Vollmer, *Optical Properties of Metal Clusters* (Springer, New York, 1995).
 - [12] G. Mie, *Ann. Phys.* **25**, 377 (1908).
 - [13] J. I. Gersten and A. Nitzan, in *Surface Enhanced Raman Scattering* (ed. R. K. Chang and T. Furtak, Plenum, New York, 1982), p 89.
 - [14] R. Jin, Y. W. Cao, C. A. Mirkin, K. L. Kelly, G. C. Schatz, J. G. Zheng, *Science* **294**, 1901 (2001).

- [15] H. Raether, *Surface Plasmons on Smooth and Rough Surfaces and on Gratings* (Springer, Berlin, 1988).
- [16] A. Otto, *Z. Phys.* **216**, 398 (1968).
- [17] B. Fischer, N. Marschall, and H. J. Queisser, *Surf. Sci.* **34**, 50 (1973).
- [18] E. N. Economu, *Phys. Rev.* **182**, 539 (1969).
- [19] D. Sarid, *Phys. Rev. Lett.* **47**, 1927 (1981).
- [20] Y. J. Chen, E. S. Koteles and R. J. Seymore, *Solid State Comm.* **46**, 95 (1983).
- [21] W-q Mu, D. B. Buchholz, M. Sukharev, R. P. H. Chang, and J. B. Ketterson (submitted).
- [22] T. Okamoto, F. H'Dhili and S. Kawata, *App. Phys. Lett.* **85**, 3968 (2004).
- [23] N. L. Dmitruk and A. V. Korovin, *Opt. Lett.* **33**, 893 (2008).
- [24] A. Hessel and A. A. Oliner, *App. Opt.* **4**, 1275 (1965).
- [25] A. Taflove and S. C. Hagness, *Computational Electrodynamics: The Finite-Difference Time-Domain Method*, 3rd ed. (Artech House, Boston, 2005).
- [26] J.-P. Berenger, *J. Comput. Phys.* **114**, 185 (1994).
- [27] M. Sukharev, J. Sung, K. G. Spears, and T. Seideman, *Phys. Rev. B* **76**, 184302 (2007).
- [28] J. Steidtner and B. Pettinger, *Phys. Rev. Lett.* **100**, 236101 (2008).
- [29] G. G. Nenninger, P. Tobiska, J. Homola, S. S. Yee, *Sensors and Actuators B* **74**, 145 (2001).

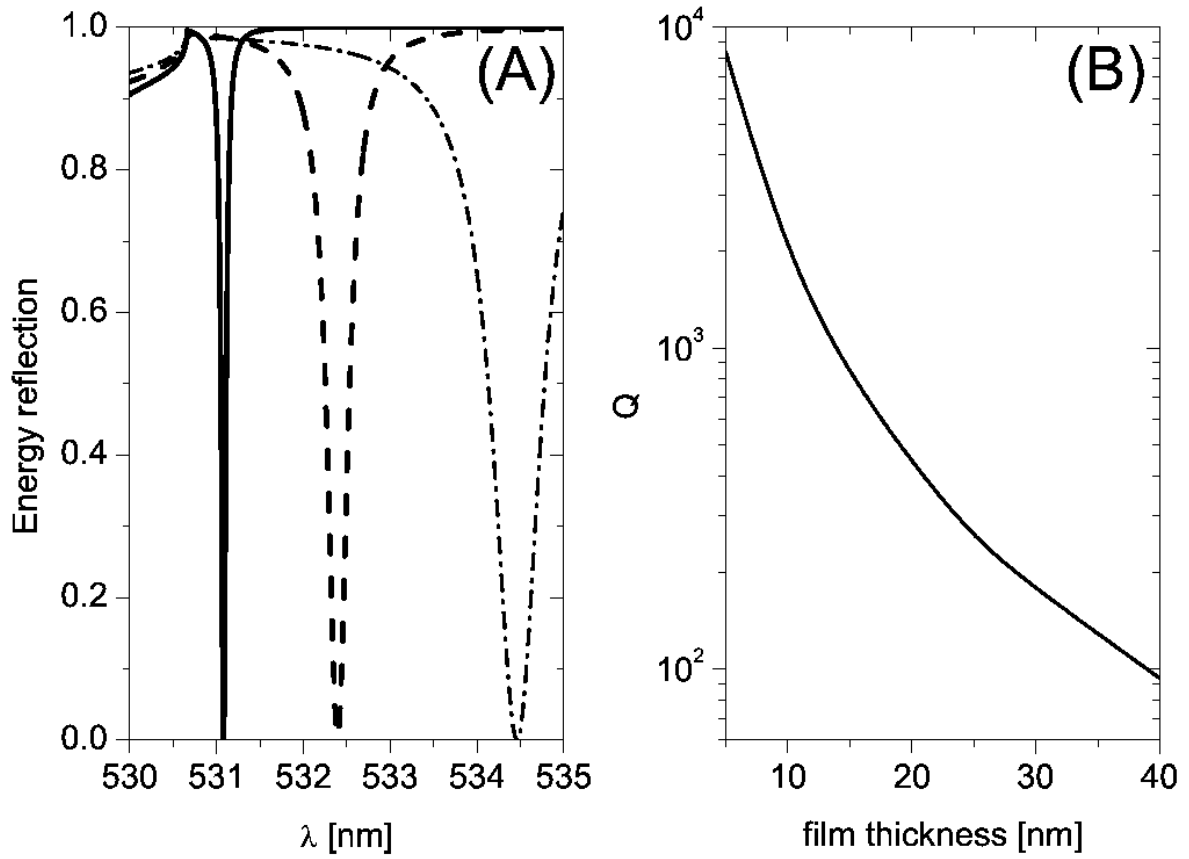


FIG. 1: (A) Energy reflection coefficient vs wavelength at critical coupling for film thicknesses of 5 nm (solid curve), 10 nm (dashed curve), and 15 nm (dash-dotted curve). (B) Quality factor, $Q = \lambda/\Delta\lambda$, for the surface plasmon resonance vs silver film thickness derived from the linewidths shown in Fig. 1A.

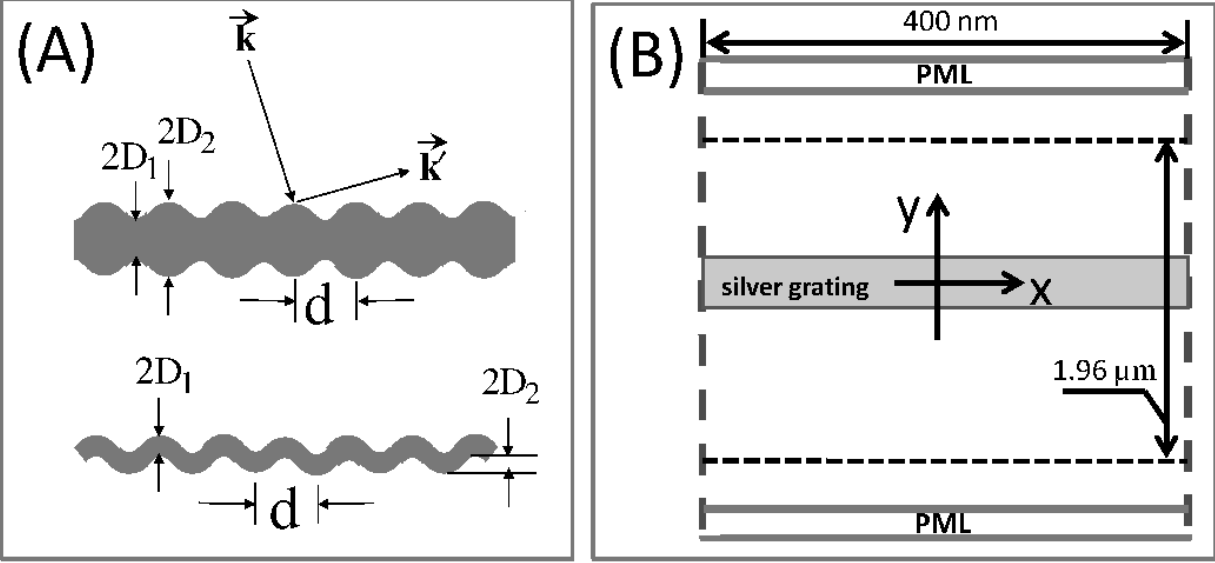


FIG. 2: (A) Schematic setup of out-of-phase and in-phase sinusoidal gratings. (B) Unit cell of FDTD simulations. The vertical dashed lines depict the periodic boundaries. Two horizontal dashed lines represent the detection contours. The metal film shown in the center of the unit cell is excited either by a laser pulse generated along a single horizontal line placed a few spatial steps beneath the upper PML region (we refer to this excitation scheme as a single-ended excitation), or by two incident plane waves generated symmetrically on both sides of the film with a fixed phase delay between the incident pulses (referred to as double-ended excitation scheme).

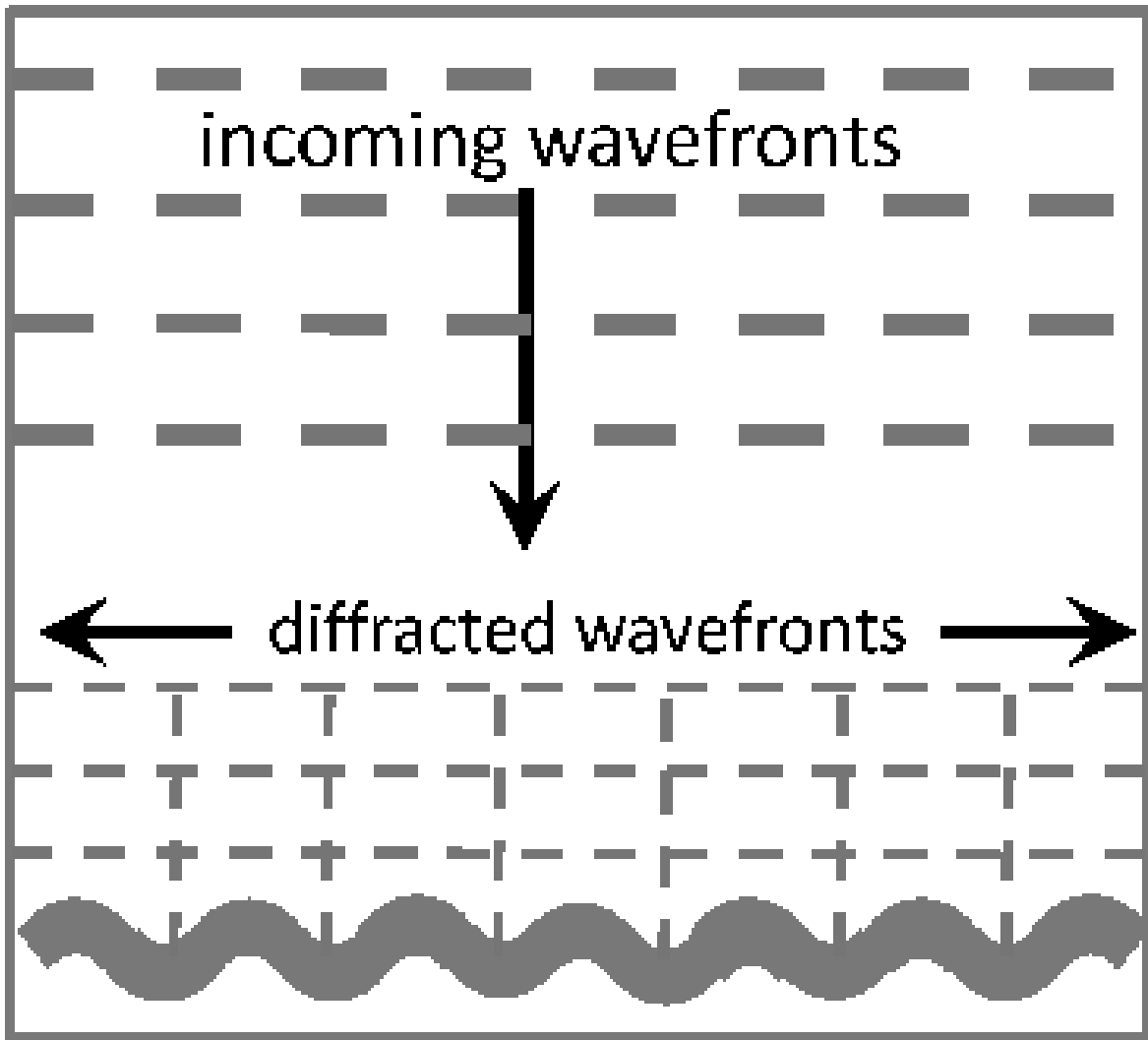


FIG. 3: The electromagnetic Wood's phenomenon in which an incoming wave (entering perpendicular) is diffracted tangent to the grating such that the wave fronts match the grating spacing resulting in anomalies in the reflected and transmitted waves.

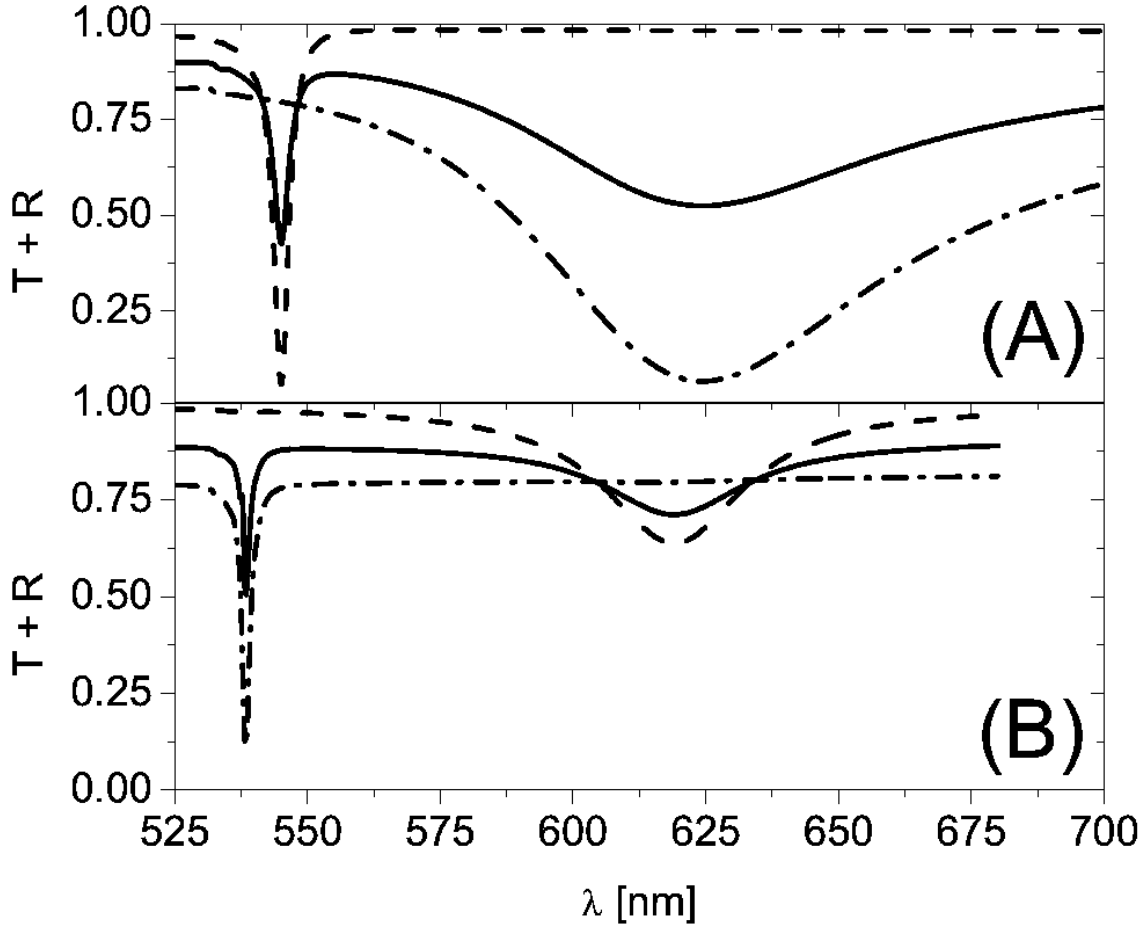


FIG. 4: Sum of the transmission, T , and reflection, R , coefficients as a function of the incident wavelength. The solid curve illustrates the single-ended excitation scheme, whereas the dashed and dash-dotted curves show the double-ended excitation with phase shifts π and 0. Panel A corresponds to the out-phase sinusoidal grating with $D_1 = 5$ nm and $D_2 = 31$ nm. Panel B shows data for the in-phase sinusoidal grating with parameters $D_1 = 10$ nm and $D_2 = 14.4$ nm. The structural parameters for both gratings have been optimized so as to minimize $T+R$ for the double ended excitation scheme and the long-range mode. (Panel A - dashed curve, panel B - dash-dotted curve).

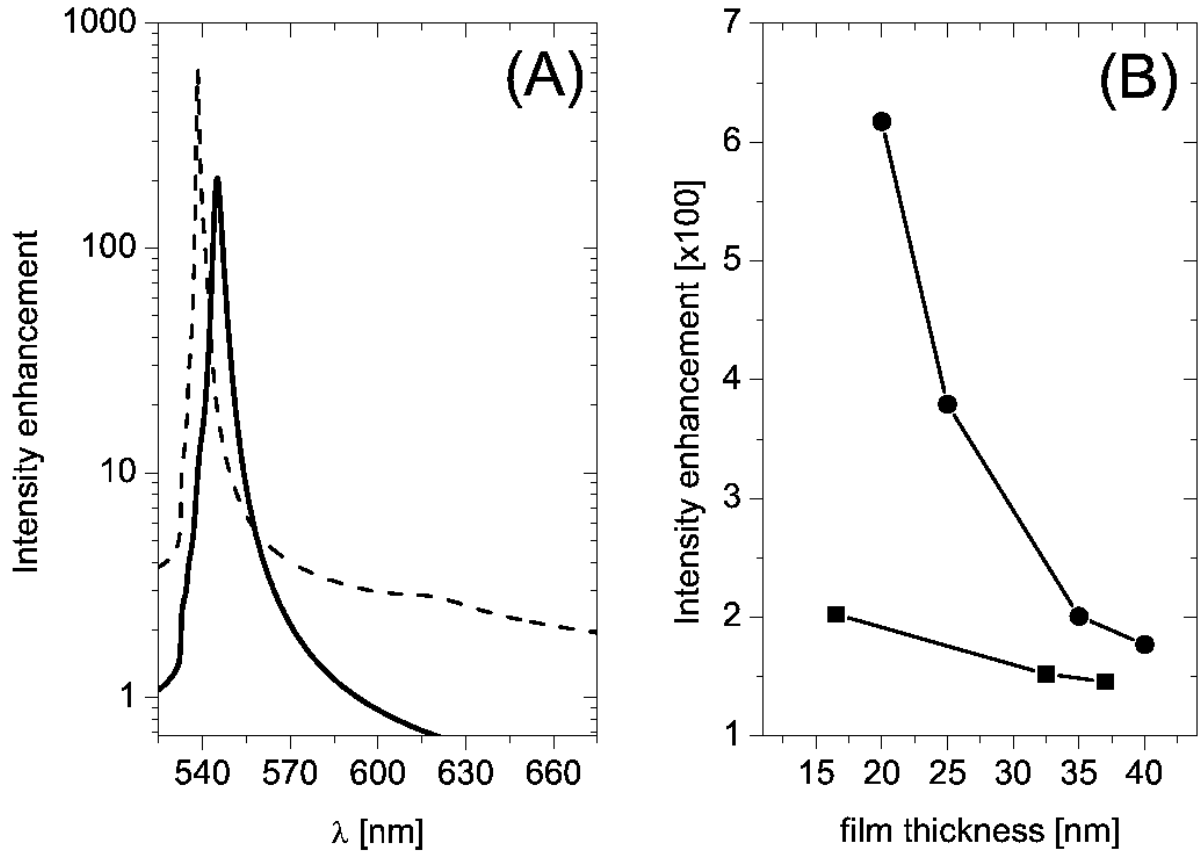


FIG. 5: (A) Surface averaged intensity enhancement as a function of the incident wavelength for out-of-phase (solid curve) and in-phase (dashed curve) gratings at the impedance matching conditions for the long-range plasmon mode. (B) Surface averaged intensity enhancement as a function of the film thickness at the impedance matching conditions for long-range plasmon modes for the out-of-phase (squares) and in-phase (circles) sinusoidal grating.